Materials Science and Engineering B 172 (2010) 146–150

Contents lists available at ScienceDirect

Materials Science and Engineering B

journal homepage: www.elsevier.com/locate/mseb

Critical length and giant magnetoimpedance in $Co_{69}Fe_{4.5}Ni_{1.5}Si_{10}B_{15}$ amorphous ribbons

Anurag Chaturvedi[a], Tara P. Dhakal[a], Sarath Witanachchi[a], Anh-Tuan Le[b], Manh-Huong Phan[a,*], Hariharan Srikanth[a]

[a] Department of Physics, University of South Florida, Tampa, FL 33620, USA
[b] Hanoi Advanced School of Science and Technology (HAST), Hanoi University of Technology, 01 Dai Co Viet street, Hanoi, Viet Nam

ARTICLE INFO

Article history:
Received 26 January 2010
Received in revised form 26 April 2010
Accepted 28 April 2010

Keywords:
Amorphous ribbons
Length effect
Magnetoimpedance
Magnetic sensors

ABSTRACT

We report a systematic study of the influence of sample length on the giant magnetoimpedance (GMI) effect and its field sensitivity (η) in $Co_{69}Fe_{4.5}Ni_{1.5}Si_{10}B_{15}$ amorphous ribbons in the frequency range of 0.1–10 MHz. We show that there exists a critical length ($L_0 \sim 8$ mm) below which the maximum GMI and η decrease with decreasing sample length (L) and above which they increase with decreasing L. The critical frequency, at which the maximum GMI and η are achieved, reaches the largest value for samples with $L = L_0$ and shifts to lower values for samples with $L < L_0$ and $L > L_0$. Our observations provide important practical guidance for optimization of the geometrical dimensions of magnetic sensing elements and design of GMI-based magnetic sensors. The demagnetization contribution for $L < L_0$ and the origin of the existence of L_0 and f_0 are discussed in the context of the permeability and resistance dependences of GMI.

1. Introduction

Research on soft ferromagnetic materials exhibiting giant magnetoimpedance (GMI) effect for high-performance magnetic sensors is an area of topical interest [1]. The GMI effect is defined as the large change of the ac impedance of a magnetic material when a dc magnetic field is applied. GMI has been observed in a variety of materials, such as magnetic wires [2], ribbons [3] and thin films [4], and it strongly depends on the geometrical dimensions of the samples [5–10]. However, for practical applications that require fabrication of sensors of different dimensions, the sample length (L) dependence of GMI in different types of samples needs further investigation. Vazquez et al. [11] reported that the GMI effect decreased in Fe-based nanocrystalline wires as the wire length decreased from 8 to 1 cm. A similar trend was also observed for the case of Co-based amorphous ribbons [12–14], Fe-based nanocrystalline ribbons [15,16] and CoSiB/Cu/CoSiB layered thin films [5]. However, Phan et al. [17] reported that the decrease of length of a Co-based microwire from 4 to 1 mm resulted in a strong increase of the GMI effect. These varied observations lead to a general expectation that for each type of material there exists a critical length (L_0), below which the GMI effect decreases with decreasing sample length [11–15] and above which it increases with decrease of sample length [17]. This hypothesis has been supported by the previous observation of the effect of L_0 on the magnetization process in Co-based and Fe-based amorphous wires [18]. It has been shown that the spontaneous magnetic bistability of these wires is lost when the sample length becomes less than the critical length ($L < L_0$). In this case, the authors have attributed the loss of magnetic bistability to the influence of shape anisotropy, where for short wires the demagnetizing field became large enough to overcome the original domain structure of the sample [18]. Such modification in the domain structure near the extremities of the sample can result in variation in GMI features with respect to change in sample length. The decrease of GMI with decreasing L for the cases of Fe-based nanocrystalline wires [11] and Co-based amorphous ribbons [12–14] can be attributed to the formation of closure domain structures due to the demagnetization effect, when the measured sample length is less than the critical length, $L < L_0$. On the other hand, the increase of GMI effect with decreasing L for the case of Co-based microwires reported by Phan et al. [17] can be reconciled with the fact that the measured sample length is larger than the critical length, $L > L_0$. For practical applications in sensors and actuators based on GMI effect, there is an emerging need for a clear understanding of the sample length dependence of GMI in a single material.

We present here a comprehensive study of the influence of sample length ($L = 2$, 5, 8, and 10 mm) on the GMI effect and

* Corresponding author. Tel.: +1 813 974 4714.
E-mail addresses: tuanla-hast@mail.hut.edu.vn (A.-T. Le), phanm@usf.edu (M.-H. Phan), sharihar@usf.edu (H. Srikanth).

0921-5107/$ – see front matter © 2010 Elsevier B.V. All rights reserved.
doi:10.1016/j.mseb.2010.04.038

magnetic sensitivity parameter (η) (to be defined in the next section) in $Co_{69}Fe_{4.5}Ni_{1.5}Si_{10}B_{15}$ amorphous ribbons over a frequency range of 0.1–10 MHz. Our studies show that there exists a critical length ($L_0 \sim 8$ mm) in the $Co_{69}Fe_{4.5}Ni_{1.5}Si_{10}B_{15}$ amorphous ribbons, for which the largest GMI and η are achieved. Below the critical length ($L < L_0$), the GMI and η decrease with decreasing L, resulting from the possible formation of closure domain structures near the ends of the sample governed by the demagnetization effect. Above the critical length ($L > L_0$), the increase of GMI effect and η with decreasing L can be attributed to the decrease of electrical resistance. We also find that the critical frequency (f_0), at which the maximum GMI and η are achieved, reaches the largest value for samples with $L = L_0$ and shifts to lower values for samples with $L < L_0$ and $L > L_0$. These findings point to the importance of the geometrical dimensions of samples and provide some insights for optimizing the GMI effect in highly sensitive GMI-based magnetic sensors.

2. Experimental

Amorphous $Co_{69}Fe_{4.5}Ni_{1.5}Si_{10}B_{15}$ ribbons with a width of 1 mm and a thickness of 16 μm were prepared by the melt-spinning method. In this technique, the purity elements were firstly put in a quartz crucible, evacuated to a high vacuum state, then filled the crucible with highly purified argon and melted them at appropriate temperature in 5 min. The obtained ingots with a certain composition were then put into a quartz tube orifice and melted by heated high frequency induction coils wound around the tube. The jet located distance from the surface of cooling copper drum ~0.3 mm with a sloping angle $\theta \sim 1$–2°. Under pressure (~0.2 MPa), a jet of the molten alloy was injected from the orifice into the surface of a cooling copper wheel, which was rotating at a longitudinal speed of 30 m s^{-1} in Ar. The width and thickness of amorphous ribbon was controlled by tuning the dimensions of the orifice, the drum velocity, and the injection pressure. The amorphous nature of the as-quenched ribbons was examined by X-ray diffraction (XRD) and the atomic percentages of the elements were established by inductive coupled plasma spectroscopy [19]. The surface topography of the ribbon sample was analyzed using a Digital Instruments Dimension 3100 Atomic Force Microscope. The ribbon samples of different lengths of $L = 2$, 5, 8 and 10 mm were used for the present study. These samples were from the same ribbon length. Field dependent magnetization (M–H) measurements were performed at room temperature using a Physical Property Measurement System (PPMS) from Quantum Design. In these measurements, the dc magnetic field was applied parallel to the ribbon plane and in the longitudinal direction of the ribbon. Magnetoimpedance measurements were carried out along the ribbon axis in applied dc magnetic fields up to 120 Oe over a frequency range of 0.1–10 MHz with the ac current directed along the ribbon axis. The Helmholtz coil (diameter, 30 cm) produced the dc magnetic field (H_{dc}) that is perpendicular to the ac magnetic field (H_{ac}) generated by the applied ac current. The Helmholtz coil was designed and fabricated in-house and was calibrated for the field produced against the applied current. A power supply (Kepco Instruments) was used to source the dc current in the Helmholtz coil to generate the desired magnetic field. An impedance analyzer (HP4192A) was used in the four-terminal contact mode to measure the absolute value of the impedance (Z) of the sample at room temperature. A low-noise, shielded accessory test lead (Agilent 16048G) was used to connect the sample to the impedance analyzer. All the electronic instruments were controlled using LabView. A schematic diagram of the magnetoimpedance measurement system is described in Fig. 1.

From the measured impedance, the percentage change of magnetoimpedance (i.e., the GMI ratio) with applied magnetic field is

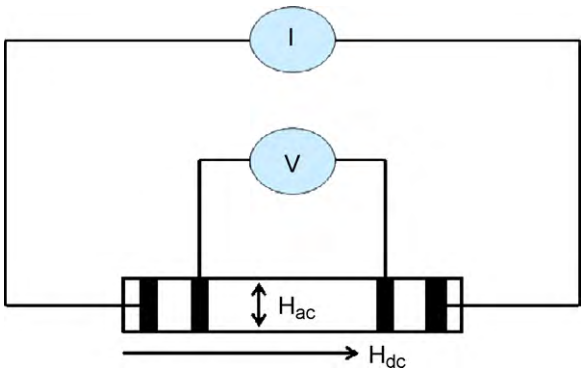

Fig. 1. Schematic view of the experimental method for measuring GMI.

expressed as

$$\frac{\Delta Z}{Z}(\%) = 100\% \times \frac{Z(H) - Z(H_{max})}{Z(H_{max})} \quad (1)$$

, and the dc magnetic field sensitivity of GMI as

$$\eta = 2 \times \frac{[\Delta Z/Z(\%)]_{max}}{\Delta H}, \quad (2)$$

where H_{max} is the maximum applied dc magnetic field to saturate the impedance of the ribbon. ΔH is a measure of the full width at half maximum (FWHM). These two parameters are the main figures of merit that we monitor for the series of samples measured and on which the analysis of the sensor response can be determined.

3. Results and discussion

Fig. 2 shows the XRD pattern of the $Co_{69}Fe_{4.5}Ni_{1.5}Si_{10}B_{15}$ as-quenched ribbon. It is clear that the pattern exhibited only one broad peak around $2\theta = 45^\circ$, which is often known as a diffuse halo, indicating that the sample prepared is nearly amorphous in nature.

Fig. 3 shows the AFM images of the surface topography of the $Co_{69}Fe_{4.5}Ni_{1.5}Si_{10}B_{15}$ amorphous ribbon sample for both surfaces. Herewith the free surface of the ribbon was that had no contact with the surface of the copper wheel (see the upper panel of Fig. 3) and the wheel-side ribbon surface was that had direct contact with the surface of the copper wheel (see the lower panel of Fig. 3). The AFM image indicates the distribution of protrusions with very high and uniform density for the free surface of the ribbon, unlike in the case of the wheel-side surface of the ribbon. The root mean squared (rms) surface roughness ($R_q = (1/n^2)\sqrt{\sum_{i=1}^{n} z_i^2}$, where z

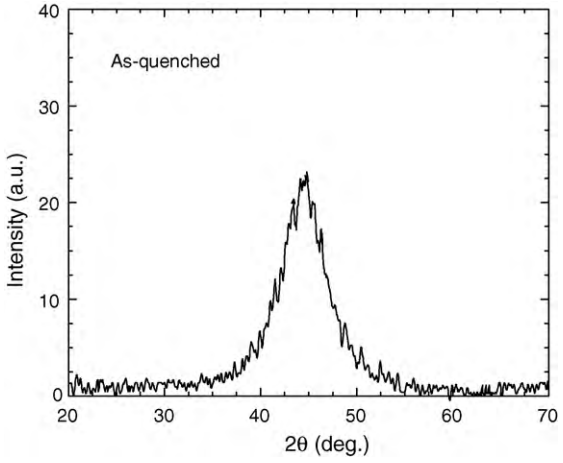

Fig. 2. The XRD pattern of the $Co_{69}Fe_{4.5}Ni_{1.5}Si_{10}B_{15}$ as-quenched amorphous ribbon.